AIAA JOURNAL
Vol. 34, No. 7, July 1996

Investigation of the Mixing Flow Structure in Multilobe Mixers

Yeng-Yung Tsui* and Po-Wenn Wu†
National Chiao Tung University, Hsinchu 300, Taiwan, Republic of China

A computational procedure is described to study the mixing flow in a multilobe turbofan mixer. The predictions have been obtained using a finite volume method to solve the density-weighted time-averaged Navier–Stokes equations. Turbulence is characterized by the k–ϵ eddy viscosity model. To fit the irregular boundaries of the flowfield, curvilinear nonorthogonal coordinates are employed. The robustness of the computational procedure is enhanced by making use of nonstaggered grids. In the calculation the computational domain contains not only the mixing duct but also the lobe itself. Three kinds of configuration are under consideration: a confluent mixer, a convoluted mixer, and a forced mixer. Results show that the streamwise vortex generated at the trailing edge is the most prominent flow structure for the forced mixer, responsible for the effective mixing. The strength of the streamwise vortex can be characterized by the circulation. A parameter termed mixedness is defined to describe the effects of the mixing process. In addition to the streamwise vortex, normal vortices are generated by the velocity difference in the shear layer between the core and fan streams. To illustrate the mechanism of the mixing procedure, velocity vectors and contours of streamwise and normal vorticities and turbulence contours on transverse planes at selected axial locations are presented. The roles played by the streamwise vortex and the normal vortex are clearly identified.

Nomenclature

$\mathrm{Cof}(\partial z_i/\partial \xi_k)$	= cofactor of $(\partial z_i/\partial \xi_k)$ in the Jacobian of the transformation $z_i = z_i(\xi_k)$
J	= Jacobian of transformation
L	= lobe length
r_k	= r, $i = 1, 2$ (i.e., $z_i = z, r$); 1, $i = 3$ (i.e., $z_i = \theta$)
S_ϕ	= source term of the ϕ transport equation
U	= velocity in the axial direction
U_i	= contravariant velocity in the ξ_i direction
z, r, θ	= axial, radial, and azimuthal directions, respectively
z_i	= cylindrical coordinates
α, β, γ	= metric coefficients of the domain transformation
Γ_ϕ	= diffusion coefficient of the ϕ transport equation
ξ_i	= curvilinear coordinates
ρ	= density
σ_0	= variance at the lobe exit
ϕ	= dependent variable
Ω	= underrelaxation factor
ω	= vorticity

Subscripts

i, j, k	= nodal indices

Superscripts

$n, n+1$	= iteration indices

I. Introduction

THE lobed mixer is an efficient device used to promote mixing of two streams in a short distance. In turbofan engines the hot flow emerging from turbine is mixed with the cold bypass flow before discharging through the nozzle. This process leads to uniform distribution of velocity and temperature and results in improvement of engine thrust and reduction in noise.[1–3]

The multilobe mixer can be regarded as an annular splitter with convoluted trailing edge (see Fig. 1). The convoluted end of the mixer increases the interfacial area between the core and the fan streams. Equally, it induces a number of counter-rotating streamwise vortices downstream of the lobes. The enhanced mixing is directly attributable to the enlarged mixing scales by the vortex flows.

The overall performance of mixers is reported in Refs. 1–3. With the use of laser Doppler velocimetry (LDV) Paterson[4] provided detailed measurements in the mixing duct. Results from his experiments showed strong vortex flows formed in the mixing duct. The vortices possessed scales on the order of the lobe size.

In the study of Werle et al.[5] dye injection was used to visualize the flow structure of the vortex generated by the forced mixer. Both laminar and turbulent flows were considered. In the laminar flow tests it was easy to observe the three stages involved in the mixing process: formation, intensification, and breakdown of the streamwise vortices.

The three-step process observed by Werle et al.[5] was confirmed in the LDV measurements of Eckerle et al.[6] The turbulence increased sharply in the first stage, slightly declined in the second stage, and was enhanced again in the last stage when the vortices broke down.

The aforementioned studies indicated that the flowfield was dominated by the large-scale, secondary vortex structure, which is responsible for the enhanced mixing. It should be recognized that the core flow velocity is usually higher than that of the fan stream. Because

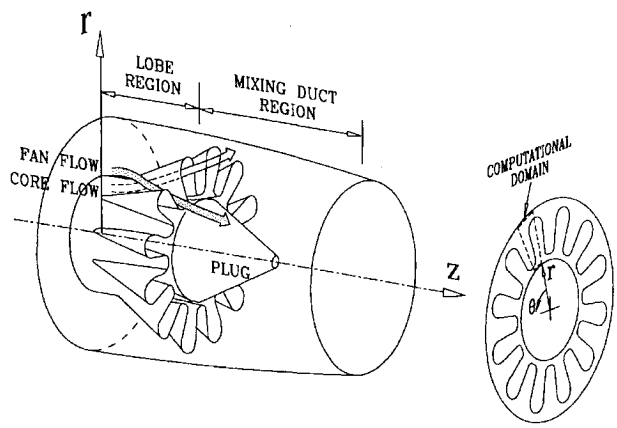

Fig. 1 Flow in the multilobe mixer.

Received Oct. 14, 1995; revision received Feb. 13, 1996; accepted for publication Feb. 20, 1996.

*Associate Professor, Department of Mechanical Engineering.
†Graduate Student, Department of Mechanical Engineering.

of the velocity difference normal vortices (normal to the streamwise direction) are shed from the trailing edge of the lobes. The work of Manning[7] revealed that the mixing enhancement increased with an enlarged velocity difference between the two streams. This implies that the normal vortex helps to enhance mixing. The flow visualization of McCormick and Bennett[8] confirmed that the streamwise vortices interacted with the normal vortices, and the structure of the normal vortex was discussed in this study.

Early attempts of numerically simulating the flow were restricted to the mixing duct (i.e., in the region downstream of the lobes) and used the parabolized Navier–Stokes (PNS) solver.[9,10] These studies emphasized that reasonable flow fields could only be obtained if sufficient details at the lobe exit were provided. To remove this difficulty and the limitations imposed by the PNS, attempts have been made to use full Navier–Stokes analyses to model the flow in the lobes together with the mixing duct. Koutmos and McGuirk[11] were the first to carry out this simulation. However, cylindrical coordinates were employed in their calculations. This prevented the boundaries from being fitted to the grid lines, and special treatments were required at boundaries. Malecki and Lord[12] and Abolfadl and Sehra[13] successfully incorporated body-fitted curvilinear grids in their models. Both studies obtained good agreement with experiments in terms of global performance parameters and temperature distribution.

In a previous study by Tsui et al.[14] a numerical procedure was developed to examine the flow in the mixing duct. Validation of the procedure was made by comparing the predictions with the data of Paterson.[4] Good agreement was obtained. In the present study the model is extended such that the computational domain can cover the lobe region. A major modification to the numerical method is the way the pressure equation is treated. Another important effort is to generate three-dimensional grids to fit the extremely irregular lobe geometries. To illustrate the effects of the streamwise vortex on the mixing in a confluent mixer, a convoluted mixer and a forced mixer are tested.

II. Mathematical Model

To deal with the complicated lobe geometry the governing equations are written in curvilinear coordinates ξ_i as

$$\frac{1}{Jr}\frac{\partial}{\partial \xi_i}(\rho U_i \phi) = \frac{1}{Jr}\frac{\partial}{\partial \xi_i}\left(\frac{\Gamma_\phi}{Jr}\frac{\partial \phi}{\partial \xi_j}B_j^i\right) + S_\phi \tag{1}$$

Here B_j^i represents the following product:

$$B_j^i = \beta_k^i \beta_k^j$$

where

$$\beta_k^i = r_k\left(\mathrm{Cof}\frac{\partial z_i}{\partial \xi_k}\right)$$

Detailed expressions for each transport equation can be found in Ref. 14.

To model turbulent effects the high Reynolds number k–ϵ model[15] was employed. The empirical constants used, found to give good agreement in a wide range of shear flows, are $C_\mu = 0.09$, $C_1 = 1.44$, and $C_2 = 1.92$. Since the generation of the secondary flow is basically an inviscid phenomenon[4,10] and the mixing process actually takes place in the shear layer between the two internal streams, it is likely that improved turbulence models such as the Reynolds stress model are unnecessary. The study of Kreskovsky et al.[16] indicated that by adopting the k–ϵ model and a rather simple viscosity model the results were insensitive to the choice of models. The use of this model was further justified in the computations of Tsui et al.[14] in which good agreement in terms of mean velocity and turbulent kinetic energy with the measurements of Paterson[4] was obtained.

The equations were discretized using the finite volume method. In the discretization the flow convection was approximated by second-order linear upwind differencing.[17] The computational grids were arranged in a nonstaggered manner and the semi-implicit method for pressure-linked equation (SIMPLE)-type iterative method[18] was

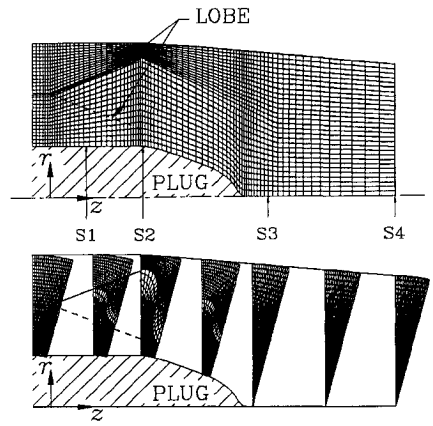

Fig. 2 Typical mesh used in the calculation.

used to deal with the coupling between the continuity and the momentum equations. It is well known that incorporating the nonstaggered grid arrangement in the SIMPLE algorithm would lead to decoupling between the pressure and velocity and thus produce checkboard oscillations.[18] To avoid this problem the momentum interpolation method of Rhie and Chow[19] was employed to calculate the velocities across cell faces. Following the SIMPLE algorithm, the face velocities were forced to satisfy the continuity constraint, and thus a pressure-correction equation was obtained. During solution iteration, a common practice[19] was to drop the corner-point contributions in the pressure-correction equation such that only seven main points were introduced in the computational template for three-dimensional problems. This practice largely simplifies the discrete equations. However, as the grid skewness increases, the weighting of the corner points increases. It can be seen from the grid shown in Fig. 2 that the grid lines deviate from the cylindrical coordinate system in the region near the lobe surface. This serious nonorthogonality may prevent the solution from converging. To remedy this problem the full pressure-correction equation was solved without any simplification, as suggested by Peric.[20] Thus, the total number of points contained in the computational template was 19. In the calculation the three-dimensional seven-point strongly implicit procedure of Stone[21] was adopted as the basic iterative solver. Those corner-node contributions were absorbed in the source term and updated after each sweep of relaxation.

Another main effort in this study was to generate a suitable three-dimensional grid to cover the entire flow domain, including the lobe region. The grid was constructed by first generating a two-dimensional grid in each transverse plane at selected axial locations and then stacking all of the two-dimensional grids to form the three-dimensional grid. The two-dimensional grids were obtained by solving the transformed Poisson equations[22] individually in the fan and core zones:

$$\alpha x_{\xi\xi} - 2\beta x_{\xi\eta} + \gamma x_{\eta\eta} = -J^2(Px_\xi + Qx_\eta) \tag{2}$$

$$\alpha y_{\xi\xi} - 2\beta y_{\xi\eta} + \gamma y_{\eta\eta} = -J^2(Py_\xi + Qy_\eta) \tag{3}$$

For a domain bounded by $\xi = 0$ and $\xi_{\max}$, and $\eta = 0$ and $\eta_{\max}$, the distribution functions

$$P(\xi,\eta) = p_1(\eta)e^{-a\xi} + p_2(\xi)e^{-b\eta} + p_3(\eta)\exp[c(\xi_{\max} - \xi)] + p_4(\xi)\exp[-d(\xi_{\max} - \xi)] \tag{4}$$

$$Q(\xi,\eta) = q_1(\eta)e^{-a\xi} + q_2(\xi)e^{-b\eta} + q_3(\eta)\exp[c(\xi_{\max} - \xi)] + q_4(\xi)\exp[-d(\xi_{\max} - \xi)] \tag{5}$$

are used to control clustering of grid points near boundaries. In the equations a, b, c, and d are positive constants. The coefficients p_i and q_i are determined by the specified spacing along $\xi = \text{const}$ lines between $\eta = 0$ boundary and the next grid nodes together with the given angle formed by the boundary lines and the intersected lines, as done by Steger and Sorenson.[23]

A typical grid resulted is shown in Fig. 2. Note that a cylindrical grid is used in the mixing duct downstream of the central plug. In the region between the lobe exit and the plug end an open boundary extended from the trailing edge of the lobe is specified to separate the domain into two zones such that the interface can gradually change from the convoluted shape to a circular shape. By using the method described earlier the grid points on boundaries change their positions during relaxation to yield a suitable grid. For the open common boundary there exists a constraint that the grid points defining this boundary in the two zones must match up. To solve this problem, an iteration between the two zones was undertaken; the grid points on the common boundary generated in one zone were imposed as given boundary points for the other zone to fulfill grid generation in this zone. Coincident points on the open common boundary were obtained when the iterative process converged.

After completing the two-dimensional grids, the corresponding grid points on all of the transverse planes were linked together to form a three-dimensional grid. However, the grid lines in the axial direction might not be smooth. Therefore, a slight adjustment of the x and y coordinates was undertaken:

$$x_{i,j,k}^{n+1} = \Omega x_{i,j,k}^{n} + (1-\Omega)\tfrac{1}{2}\left(x_{i,j,k+1}^{n+1} + x_{i,j,k-1}^{n+1}\right) \tag{6}$$

$$y_{i,j,k}^{n+1} = \Omega y_{i,j,k}^{n} + (1-\Omega)\tfrac{1}{2}\left(y_{i,j,k+1}^{n+1} + y_{i,j,k-1}^{n+1}\right) \tag{7}$$

As seen from the preceding equation, an implicit relaxation procedure was used. A value of 0.9 was taken for the underrelaxation factor Ω. Usually, not more than 40 iterations are enough to fulfill the smoothing procedure.

III. Results and Discussion

The configuration tested is shown in Fig. 1, in which a 12-lobe nozzle is included. Because of geometric periodicity and flow symmetry only half a lobe of 15 deg was necessary in the calculations. In the tests the mass flow rates on the fan and core sides were 1.84 and 2.36 kg/s, with corresponding inlet velocities of 45 and 90 m/s. At the inlet the velocity profiles were assumed uniform. The turbulence was about 6% of the inlet velocity. The length scale was chosen as a fraction of the inlet height.

As introduced previously, the streamwise vortex plays an important role in the mixing process. In the results presented next the strength of this vortex is characterized by circulation defined by

$$\Gamma = \oint_C \boldsymbol{V} \cdot \mathrm{d}\boldsymbol{S} \tag{8}$$

where the circuit C is the outer path of the computational domain, as denoted by the dashed lines given in Fig. 1. Since velocities vanish on the solid walls, the circulation is equal to the line integral of the radial velocity along the two symmetry boundaries. By the Stokes' theorem the circulation is also equivalent to the area integration of the streamwise component of vorticity in the considered cross section:

$$\Gamma = \oint_A \omega_z \, \mathrm{d}A \tag{9}$$

To evaluate the performance of mixing, a mixedness is defined. Consider the distribution of an entity ϕ over a cross-sectional area of the mixing duct. A variance, standing for the deviation from the mean value, is given by

$$\sigma = \frac{\int_A |\phi - \bar{\phi}| \, \mathrm{d}A}{\int_A \phi \, \mathrm{d}A} \tag{10}$$

where

$$\bar{\phi} = \frac{\int_A \phi \, \mathrm{d}A}{\int_A \mathrm{d}A}$$

The mixedness is then defined as

$$M = (\sigma_0 - \sigma)/\sigma_0 \tag{11}$$

where σ_0 is the variance at the lobe exit.

In this series of tests three configurations are considered. Type A is a confluent mixer, type B a convoluted mixer, and type C a forced mixer. As shown in Fig. 3, the confluent mixer is just an axisymmetric annular splitter. The convoluted mixer has the same convoluted trailing edge at the lobe exit as the forced mixer. The contour of the forced mixer varies continuously in a linear manner, whereas the convoluted mixer has a drastic change of geometry in the fore part and then remains unchanged until the end. Because of the area change in the lobe the velocity ratio of the core stream to the fan stream decreases from 2:1 at the lobe inlet to 1.54 at the lobe exit.

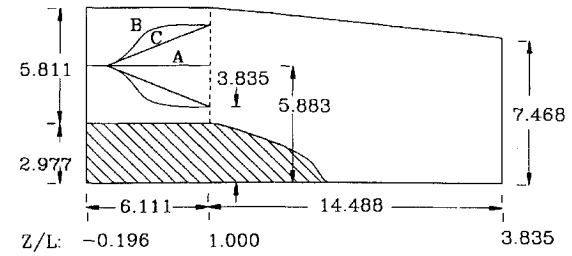

Fig. 3 Illustration of three lobe configurations tested (unit = 10^{-2} m).

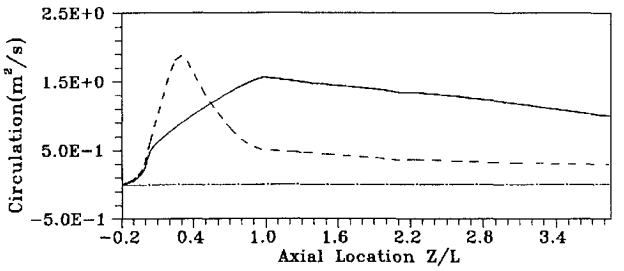

Fig. 4 Axial variation of circulation: ——, C type; – – –, B type; and — · —, A type.

A grid refinement test has been conducted for the forced mixer with node numbers ranging from 40,000 to 200,000. The predicted circulation and mixedness are not sensitive to the grid density; the differences between the computations using the two grids were less than 2%. The production of turbulence has larger dependence on the grid spacing. The deviation in terms of turbulent kinetic energy integrated over the outlet plane between the finest and the coarsest grids was about 7%. This difference is not significant yet. As will be seen, the role played by the turbulence in achieving mixing is not as prominent as the streamwise vortex flow. Therefore, the results presented in the following, obtained using a $57 \times 60 \times 22$ (z, r, θ) grid, are adequate to illustrate the mixing flow structure.

The variation of the circulation for the three cases considered is shown in Fig. 4. In this and the following figures the axial dimension is normalized using the length of the lobe, L, whereas in contour plots the velocities and turbulence intensities are nondimensionalized by the mean core velocity at the inlet (90 m/s). There is no circulation for the confluent mixer case because of the axisymmetric flow. In the convoluted mixer the circulation increases sharply at first and then quickly declines at the lobe exit, followed by a gradual attenuation in the mixing duct where the mixing process takes place. The quick decline in the lobe is ascribable to the change in lobe slope seen in Fig. 3. For the forced mixer the circulation steadily increases till the lobe exit and then gradually decreases. In the mixing duct the circulation for the forced mixer is much higher than that for the convoluted mixer.

The variation of the mixedness, defined in terms of axial velocity $(\phi = U)$, in the mixing duct is illustrated in Fig. 5. Compared with the convoluted mixer, the strong axial vortex of the forced mixer leads to enhanced mixing. The higher mixedness for the convoluted mixer than that for the confluent mixer is attributed to the appearance of the weak axial vortex and the enlarged interfacial area. The interfacial area between the core and the fan flows has been increased by a factor of 3.18 when the trailing edge is convoluted.

In Fig. 6 the axial variation of total turbulent kinetic energy integrated over each diametral plane is shown. In the confluent mixer

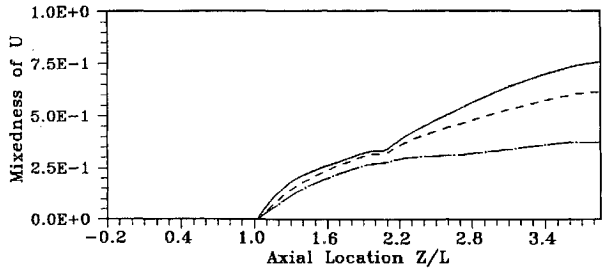

Fig. 5 Axial variation of mixedness: ——, C type; – – –, B type; and — · —, A type.

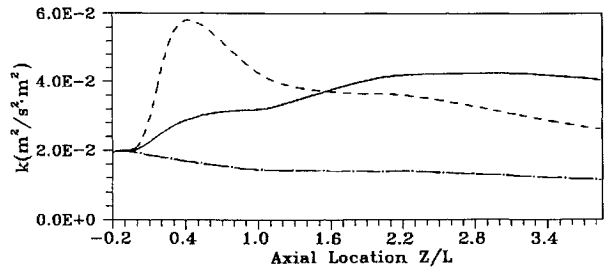

Fig. 6 Axial variation of total turbulence kinetic energy: ——, C type; – – –, B type; and — · —, A type.

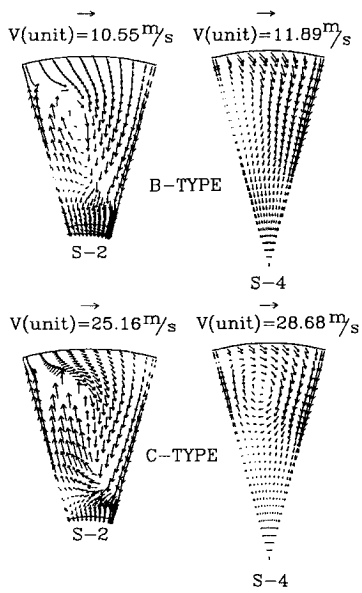

Fig. 7 Radial and angular velocity vectors in diametral planes.

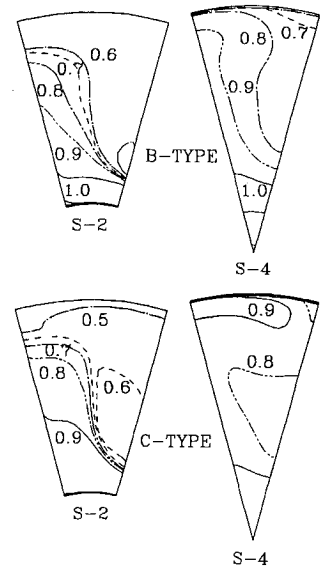

Fig. 8 Normalized axial velocity contours in diametral planes.

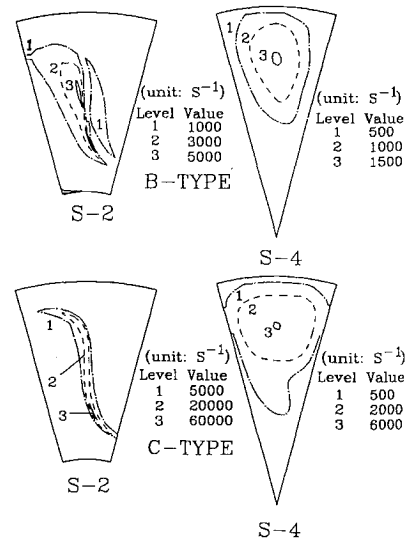

Fig. 9 Streamwise vorticity contours in diametral planes.

flow the turbulence continuously decays. For the convoluted mixer large turbulence is produced in the first part of the lobe and is followed by a steady decay. The rapid ascent of turbulence level near the lobe inlet is a result of the drastic changes of the geometry along with the cross-sectional area there, resulting in large increase in normal and axial vortices. As for the forced mixer, turbulence is produced throughout the entire lobe region until the middle of the mixing duct. Afterwards, it decays at a slow rate. Obviously, the variation of the circulation and the total turbulent kinetic energy are much alike, indicating that there exists a relation between the streamwise vorticity and the generation of turbulence. The relation will be further delineated later.

The vector plots at two z locations for the convoluted and forced mixers are shown in Fig. 7. The S2 station corresponds to the lobe exit, and the S4 is just the outlet plane (see Fig. 2). For a better illustration of the effects, the dimension in the θ direction is doubled ($\Delta\theta$ is increased from 15 to 30 deg) and the velocity vectors are drawn every other point. Because of deformation of the lobe geometry, a radially uxpward velocity is induced on the core side and a radially downward velocity on the fan side, as seen in S2 plane. After the two streams emerging from the lobe exit a vortex flow develops, as shown in the S4 plane. Comparing the convoluted mixer and the forced mixer, the secondary flow in the mixing duct for the former is much weaker, as already identified in Fig. 4.

The axial velocity contours at selected locations are presented in Fig. 8. In the mixing duct the vortex flow transports the high-speed core stream into the fan region, and by the same mechanism, the low-speed fan flow intrudes into the core region. Because of turbulent diffusion the velocity gradients are smoothed out, and thus the effective mixing is obtained in the shear layer between the two streams. The velocity distribution for the forced lobe is more uniform than that for the convoluted lobe at the outlet plane.

The gross strength of the streamwise vortex has already been characterized by the circulation in Fig. 4. Its local distribution can be represented by the contours of axial vorticity given in Fig. 9. In the lobe the induced secondary flow gives rise to large axial vorticities around the lobe surface. When the two streams mix, a well-organized vortex forms. The peak region of the vorticity roughly corresponds to the vortex center, especially for the forced mixer. The level of the vorticity is much higher for the forced mixer throughout the mixing duct.

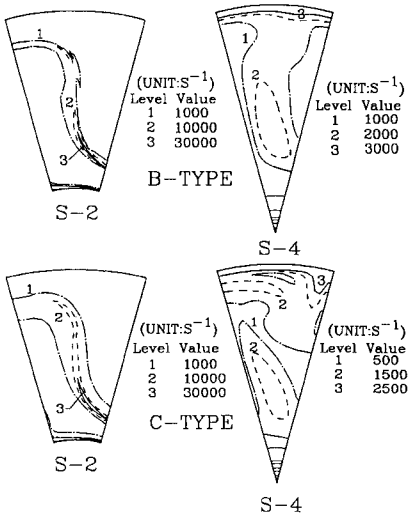

Fig. 10 Normal vorticity contours in diametral planes.

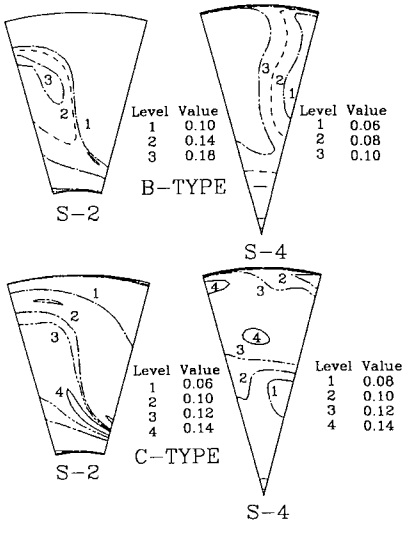

Fig. 11 Turbulence intensity contours in diametral planes.

The strength of the normal vortex, as termed by Manning,[7] can be represented by

$$\omega_n = \left(\omega_r^2 + \omega_\theta^2\right)^{\frac{1}{2}} \tag{12}$$

The normal vorticity distribution is shown in Fig. 10. It is noticed that the axial vorticities stand for the gradients of secondary flow velocities and the normal vorticities the gradients of axial velocities. As expected, the magnitudes of the normal vorticities for the two cases are alike in the entire mixing region. They are of the same order as the streamwise vorticities. It is noted that the effective mixing of the forced mixer resulting in lower normal vorticity level in the outlet plane except in the region close to the shroud.

In the contact surface of the core and fan streams, i.e., in the shear layer between the two streams, the process of mixing relies on turbulent diffusion to exchange momentum. In high-shear flows turbulence is mainly generated by shear strains. In these flows the shear strains can be characterized by vorticities. Thus the two types of vorticity discussed earlier are the main sources to produce turbulence. As seen previously, large amounts of turbulence are generated in the lobe near the inlet for the convoluted case. As a consequence, the turbulence level is higher for this case at the S2 plane (Fig. 11). Comparing the two streams indicated that larger turbulence values are obtained on the core stream side as a result of higher flow velocity. In the mixing duct, the turbulence monotonically decays in the convoluted case, whereas for the forced mixer the overall level of turbulence is promoted first and then slightly decays, which was evident in Fig. 5. At the outlet plane S4 the turbulence level is higher for the latter than for the former. The good behavior of the turbulence characteristics for the forced mixer is mainly attributable to the well-organized axial vortex.

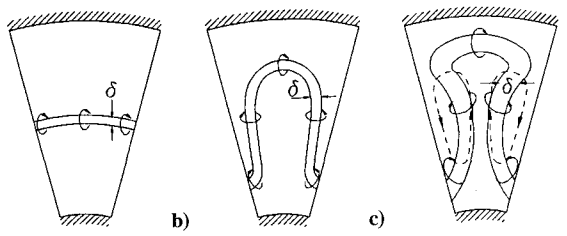

Fig. 12 Schematic illustration of the mixing process in a) confluent mixer, b) convoluted mixer, and c) forced mixer.

According to the preceding discussion, the mixing enhancement caused by the streamwise vortex can be schematically illustrated in Fig. 12. For the convoluted mixer it is assumed that there is no streamwise vortex generated. The mixing caused by the turbulent diffusion takes place in the shear layer around the projection region of the trailing edge in the mixing duct. Turbulence is generated in this layer by the normal vorticity resulting from the axial velocity difference for the confluent mixer and the convoluted mixer. Apparently, the interfacial area is largely increased by the convoluted trailing edge in the later case. When axial vortices are introduced in the forced mixer, it can be seen that the interfacial surface is distorted and, thus, further elongated by the convection transport of the rotating vortex flow. The thickness of the mixing layer is also increased because the turbulence is generated not only by the normal vorticity but also by the axial vorticity. As a result of this process the mixing region in the forced mixer is quickly spread to encompass the entire flow domain. Therefore, good mixing can be achieved in a short distance.

IV. Conclusion

A finite volume procedure, using the curvilinear nonorthogonal grid together with the nonstaggered arrangement of the nodal points, has been developed and applied to examine the flow in the multilobe mixer. A summary of main findings are as follows.

1) The effective mixing process taking place downstream of the convoluted trailing edge of the lobe is mainly caused by the streamwise vortex. The strength of the streamwise vortex can be characterized by the circulation. The mixedness is correlated to the circulation.

2) Because of the axial velocity difference normal vortices arise in the shear layer between the two streams. The magnitudes of the normal vorticity are on the same order as those of the axial vorticity. Both contribute to generate turbulence.

3) Because of convection transport by the axial vortex flow the contact surface between the two streams is distorted and its length scale is elongated. The turbulent diffusion generated by the axial vorticity and the normal vorticity helps increase the interfacial thickness. As a consequence, the mixing is quickly spread over the flowfield in the forced mixer.

Acknowledgments

This work was supported by the National Science Council under Contracts SC 83-0210-D009-30 and NSC 84-2212-E009-006.

References

[1]Crouch, R. W., Coughlin, C. L., and Paynter, G. C., "Nozzle Exit Flow Profile Shaping for Jet Noise Reduction," *Journal of Aircraft*, Vol. 14, Sept. 1977, pp. 860–867.

[2]Shumpert, P. K., "An Experimental Model Investigation of Turbofan Engine Internal Exhaust Gas Mixer Configuration," AIAA Paper 80-0228, Jan. 1980.

[3]Kozlowski, H., and Kraft, G., "Experimental Evaluation of Exhaust Mixers for an Energy Efficient Engine," AIAA Paper 80-1088, June 1980.

[4]Paterson, R. W., "Turbofan Forced Mixer-Nozzle Internal Flow Field I—A Benchmark Experimental Study," NASA CR 3492, 1982.

[5]Werle, M. J., Paterson, R. W., and Presz, W. M., Jr., "Flow Structure in a Periodic Axial Vortex Array," AIAA Paper 87-0610, Jan. 1987.

[6]Eckerle, W. A., Sheibani, H., and Awad, J., "Experimental Measurement of the Vortex Development Downstream of a Lobed Forced Mixer," *Journal of Engineering for Gas Turbines and Power*, Vol. 114, No. 1, 1992, pp. 63–71.

[7]Manning, T. A., "Experimental Studies of Mixing Flows with Streamwise Vorticity," M.S. Thesis, Dept. of Aeronautics and Astronautics, Massachusetts Inst. of Technology, Cambridge, MA, 1991.

[8]McCormick, D. C., and Bennett, J. C., Jr., "Vortical and Turbulent Structure of a Lobed Mixer Free Shear Layer," *AIAA Journal*, Vol. 32, No. 9, 1994, pp. 1852–1859.

[9]Birch, S. C., Paynter, G. C., Spalding, D. B., and Tatchell, D. G., "An Experimental and Numerical Study of the Three-Dimensional Mixing Flows of a Turbofan Engine Exhaust System," AIAA Paper 77-204, Jan. 1977.

[10]Povinelli, L. A., and Anderson, B. H., "Investigation of Mixing in a Turbofan Exhaust Duct, Part II: Computer Code Application and Verification," *AIAA Journal*, Vol. 22, No. 4, 1984, pp. 518–525.

[11]Koutmos, P., and McGuirk, J. J., "Turbofan Forced Mixer/Nozzle Temperature and Flow Field Modeling," *International Journal of Heat and Mass Transfer*, Vol. 32, No. 6, 1989, pp. 1141–1153.

[12]Malecki, R., and Lord, W., "Navier–Stokes Analysis of a Lobed Mixer and Nozzle," AIAA Paper 90-0453, Jan. 1990.

[13]Abolfadl, M. A., and Sehra, A. K., "Application of Three-Dimensional Viscous Analysis to Turbofan Forced Mixer," AIAA Paper 91-0131, Jan. 1991.

[14]Tsui, Y. Y., Wu, P. W., and Liao, C. W., "Flow Modeling in Turbofan Mixing Duct," *Numerical Heat Transfer*, Pt. A, Vol. 26, No. 2, 1994, pp. 219–236.

[15]Spalding, D. B., and Launder, B. E., "The Numerical Computation of Turbulent Flows," *Computer Methods in Applied Mechanics and Engineering*, Vol. 3, No. 3, 1974, pp. 269–289.

[16]Kreskovsky, J. P., Briley, W. R., and McDonald, H., "Investigation of Mixing in a Turbofan Exhaust Duct, Part I: Analysis and Computational Procedure," *AIAA Journal*, Vol. 22, No. 3, 1984, pp. 374–382.

[17]Tsui, Y. Y., "A Study of Upstream-Weighted High-Order Differencing for Approximation to Flow Convection," *International Journal for Numerical Methods in Fluids*, Vol. 13, No. 2, 1991, pp. 167–199.

[18]Patankar, S. V., *Numerical Heat Transfer and Fluid Flow*, McGraw–Hill, New York, 1980.

[19]Rhie, C. M., and Chow, W. L., "Numerical Study of the Turbulent Flow Past an Airfoil with Trailing Edge Separation," *AIAA Journal*, Vol. 21, No. 11, 1983, pp. 1525–1532.

[20]Peric, M., "Analysis of Pressure-Velocity Coupling on Nonorthogonal Grids," *Numerical Heat Transfer*, Pt. B, Vol. 17, No. 1, 1990, pp. 63–82.

[21]Stone, H. L., "Iterative Solution of Implicit Approximations of Multidimensional Partial Differential Equations," *SIAM Journal on Numerical Analysis*, Vol. 5, No. 3, 1968, pp. 530–558.

[22]Thompson, J. F., *Numerical Grid Generation-Foundations and Applications*, North-Holland, New York, 1985.

[23]Steger, J. L., and Sorenson, R. L., "Automatic Mesh-Point Clustering Near a Boundary in Grid Generation with Elliptic Partial Differential Equations," *Journal of Computational Physics*, Vol. 33, No. 3, 1979, pp. 405–410.